First-Principles Investigation of the Li−Fe−F Phase Diagram and Equilibrium and Nonequilibrium Conversion Reactions of Iron Fluorides with Lithium

Robert E. Doe,[†] Kristin A. Persson,[†] Y. Shirley Meng,[‡] and Gerbrand Ceder*,[†]

Department of Materials Science and Engineering, Massachusetts Institute of Technology, Cambridge, Massachusetts 02139, and Department of Materials Science and Engineering, University of Florida, Gainesville, Florida 32611

Received April 22, 2008. Revised Manuscript Received June 6, 2008

We have used density functional theory (DFT) to investigate the ternary phase diagram of the Li−Fe−F system and the reactions of Li with iron fluorides. Several novel compounds, not previously identified in the Li−Fe−F system, are predicted to be stable. Electrochemical voltage profiles, derived from the evolution of the Li chemical potential in the calculated phase diagram, are in reasonable agreement with experimental trends. The effect of particle size on the Fe that precipitates when Li_xFeF_3 reacts with Li is also investigated. We find that when 1 nm Fe particles form, the potential for this reaction is considerably reduced from its bulk value and relate this to the experimental observations. Furthermore, we formulate a model for the significant hysteresis that is observed in the lithiation and delithiation of FeF_3. Nonequilibrium paths derived by assuming much faster diffusion of Li than Fe are in reasonable agreement with experimental profiles. Our kinetic model predicts that the iron fluoride reaction follows a different path through the phase diagram during conversion (discharge) and reconversion (charge), which results in the voltage profile hysteresis observed during experiment. The proposed kinetic model also explains why upon extraction of Li from a 3/1 mixture of LiF and Fe a rutile FeF_2-like structure can form, even when iron should be oxidized to Fe^{3+} by extraction of three Li^+ per Fe.

I. Introduction

The lithium ion (Li-ion) battery has become the premier technology for portable power because of its ability to meet the ever-increasing power and energy density demands of modern electronic devices.[1] The principle by which Li-ion chemistry moves electrons through an external circuit relies upon Li^+ insertion into one electrode material while extracting Li^+ from the opposing electrode material.[2,3] Commonly referred to as the "rocking chair" mechanism, this process requires the electrodes to be composed of host materials that remain structurally and electrochemically stable during repeated charge/discharge cycles. This requirement has practically restricted the reversible reaction to at most a single electron transfer per formula unit, in turn limiting the energy density that can be achieved with current anodic (e.g., graphite) and cathodic (e.g., $LiCoO_2$, $LiNiO_2$, $LiFePO_4$) insertion materials.

An alternative to Li^+ insertion reactions is the displacement or "conversion" reaction in which the active electrode material, MX_y, is consumed by Li^+ and reduced to the metal, M^0, and a corresponding lithium compound, $Li_{zy}X$:

$$M^{z+}X_y + zLi^+ \underset{\text{discharge}}{\overset{\text{charge}}{\rightleftharpoons}} M^0 + yLi_{zy}X \qquad (1)$$

In eq 1, M represents the metal cation and X represents the anion. These reactions can make use of all energetically favorable valence states of the metal cation, enabling a large theoretical energy density. Reversible conversion reactions have been demonstrated with a variety of materials including metal oxides,[4,5] metal nitrides,[6–8] metal sulfides,[9,10] and metal fluorides.[11–15] Because the conversion reaction potential is directly proportional to the strength of the bond ionicity only metal fluorides have a high enough potential to be used as Li-ion cathodes. Although the very ionic nature of the

* Corresponding author. E-mail: gceder@mit.edu.
[†] Massachusetts Institute of Technology.
[‡] University of Florida.

(1) Brodd, R. J.; Bullock, K. R.; Leising, R. A.; Middaugh, R. L.; Miller, J. R.; Takeuchi, E. *J. Electrochem. Soc.* **2004**, *151*, K1−K11.
(2) Wakihara, M. *Mater. Sci. Eng.* **2001**, *R33*, 109–134.
(3) *Lithium Batteries: Science and Technology*, 1st ed.; Nazri, G. A., Pistoia, G., Eds.; Kluwer Academic Publishers: Boston, MA, 2004.
(4) Grugeon, S.; Laruelle, S.; Herrera-Urbina, R.; Dupont, L.; Poizot, P.; Tarascon, J. M. *J. Electrochem. Soc.* **2001**, *148*, A285.
(5) Poizot, P.; Laruelle, S.; Grugeon, S.; Dupont, L.; Tarascon, J. M. *Nature* **2000**, *407*, 496.
(6) Pereira, N.; Balasubramanian, M.; Dupont, L.; McBreen, J.; Klein, L. C.; Amatucci, G. G. *J. Electrochem. Soc.* **2003**, *150*, A1118−A1128.
(7) Pereira, N.; Dupont, L.; Tarascon, J. M.; Klein, L. C.; Amatucci, G. G. *J. Electrochem. Soc.* **2003**, *150*, A1273−A1280.
(8) Pereira, N.; Klein, L. C.; Amatucci, G. G. *J. Electrochem. Soc.* **2002**, *148*, A262−A271.
(9) Besenhard, J. O. *Z. Naturforsch., B: Chem. Sci.* **1978**, *33*, 279.
(10) Poizot, P.; Laruelle, S.; Grugeon, S.; Tarascon, J. M. *J. Electrochem. Soc.* **2002**, *149*, A1212.
(11) Badway, F.; Cosandey, F.; Pereira, N.; Amatucci, G. G. *J. Electrochem. Soc.* **2003**, *150*, A1318.
(12) Badway, F.; Mansour, A. N.; Pereira, N.; Al-Sharab, J. F.; Cosandey, F.; Plitz, I.; Amatucci, G. G. *Chem. Mater.* **2007**, *19*, 4129–4141.
(13) Badway, F.; Pereira, N.; Cosandey, F.; Amatucci, G. G. *J. Electrochem. Soc.* **2003**, *150*, A1209.
(14) Bervas, M.; Badway, F.; Klein, L. C.; Amatucci, G. G. *Electrochem. Solid-State Lett.* **2005**, *8*, A179.
(15) Li, H.; Balaya, P.; Maier, J. *J. Electrochem. Soc.* **2004**, *151*, A1878.

10.1021/cm801105p CCC: $40.75
Published on Web 07/25/2008

metal−fluorine bond produces a high reaction potential, the corresponding wide band gap results in electronically insulating behavior, which has inhibited the use of metal fluoride electrodes until recently. A variety of metal fluorides (e.g., those based on Fe, Co, Ni, Cu, Bi) exhibited significant electrochemical activity when prepared as a nanocomposite consisting of small particles (on the order of ∼1−20 nm) embedded in a conductive matrix (e.g., carbon, V_2O_5, MoS_2).[11–14] Use of fine nanoscale metal fluorides minimizes the length of the ion diffusion path while the conductive matrix serves to enhance and maintain interparticle electronic and ionic conductivity during prolonged cycling.

One well-studied metal fluoride that typifies conversion reaction behavior is iron fluoride.[11,13,16,17] It has been demonstrated that carbon metal fluoride nanocomposites containing 85/15 wt % FeF_3/C exhibit a reversible capacity of 600 mAh/g (FeF_3 theoretical capacity = 712 mAh/g) between 4.5 and 1.5 V versus Li/Li^+. This performance is roughly 4 times the specific capacity and nearly 3 times the gravimetric energy density of $LiCoO_2$. Investigation of the FeF_3 conversion mechanism by electrochemical and structural analysis has lead other authors[11,13] to ascertain that initial Li^+ insertion occurs at ∼3.3 V versus Li/Li^+ according to the reaction

$$Fe^{3+}F_3 + Li^+ \rightarrow LiFe^{2+}F_3 \quad (2)$$

This portion of the reaction has been found to take place readily and be fully reversible, whereas the subsequent step, observed at ∼2 V versus Li/Li^+, is thought[11] to correspond to the reaction

$$LiFe^{2+}F_3 + 2Li^+ \rightarrow Fe^0 + 3LiF \quad (3)$$

This segment of the overall reaction occurs with a significant voltage drop, and the amount of capacity obtained is extremely rate and temperature-sensitive. Observations such as these lead to speculation that conversion reactions are kinetically, rather than thermodynamically, hindered.[11,15,18]

Reconversion of the Fe and LiF nanocomposite to iron fluoride takes place with significant polarization, resulting in considerable hysteresis of the voltage profile, a characteristic common to many conversion reactions.[15] Reconversion of LiF and Fe is also quite intriguing because a capacity equivalent to three Li^+ per Fe is obtained although an "FeF_2-like" structure is produced instead of the initial FeF_3 structure.[11] In addition, features of the electrochemical profile for an FeF_2/C nanocomposite conversion/reconversion process appear quite similar to those obtained from charge/discharge cycles of the FeF_3/C nanocomposite (particularly cycles subsequent to the first). Since it is difficult to reconcile how three Li^+ can be extracted per Fe, when Fe is only oxidized to +2 in FeF_2, mechanisms involving interfacial or surface charge storage have been proposed.[11,15] At the present time, the details of this process are poorly understood primarily because of the analytical limitations of current experimental instrumentation encountered when examining such fine nanostructures.

The work presented herein demonstrates the application of first-principles calculations to the study of conversion reactions by specifically investigating the iron fluoride conversion mechanism. In recent years, first-principles calculations have been used to accurately predict and explain a variety of properties pertinent to Li-ion insertion materials such as average insertion potential(s),[19–24] voltage profile,[20,25–27] phase stability,[28–30] and lithium and electron mobilities.[31–33]In this paper, we use first-principles methods to investigate the stable and metastable phases in the Li−Fe−F ternary system and predict plausible reaction paths. We also explain the apparent paradox how three Li^+ can be extracted from the discharged state while forming an FeF_2-like structure upon reconversion. Finally, we also propose a model for the significant hysteresis observed in the voltage profile of iron fluoride, and for conversion reactions in general.

II. Computational Methodology and Crystal Structures

The first-principles calculations were conducted within the formalism of density functional theory (DFT) and the generalized gradient approximation (GGA) of the exchange-correlation function as formulated by Perdew, Burke, and Ernzerhof.[34] Pseudopotentials generated by the projector-augmented wave (PAW) method[35,36] were utilized as implemented by the Vienna ab Initio Simulation Package (VASP).[37] The pseudopotentials utilized the valence state $1s^12s^12p^1$ for Li, $3p^13d^74s^1$ for Fe, and $2s^22p^5$ for F. Planewave convergence to less than 5 meV/atom was achieved by using an energy cutoff of 550 eV, higher than the default value of 400 eV for fluorine, and Brillouin zone integration was performed on a 4 × 4 × 4 grid for all metal fluorides and a 12 × 12 × 12 grid for Li and Fe. Minimization of the total energy was realized with a

(16) Plitz, I.; Badway, F.; Al-Sharab, J.; DuPasquier, A.; Cosandey, F.; Amatucci, G. G. *J. Electrochem. Soc.* **2005**, *152*, A307.
(17) Cosandey, F.; Al-Sharab, J. F.; Badway, F.; Amatucci, G. G.; Stadelmann, P. *Microsc. Microanal.* **2007**, *13*, 87–95.
(18) Arico, A. S.; Bruce, P.; Scrosati, B.; Tarascon, J.-M.; Van Schalkwijk, W. *Nat. Mater.* **2005**, *4*, 366–377.
(19) Zhou, F.; Cococcioni, M.; Marianetti, C. A.; Morgan, D.; Ceder, G. *Phys. Rev. B* **2004**, *70*, 235121.
(20) Aydinol, M. K.; Kohan, A. F.; Ceder, G.; Cho, K.; Joannopoulos, J. *Phys. Rev. B* **1997**, *56*, 1354–1365.
(21) Hwang, B. J.; Tsai, Y. W.; Carlier, D.; Ceder, G. *Chem. Mater.* **2003**, *15*, 3676–3682.
(22) Kganyago, K. R.; Ngoepe, P. E.; Catlow, C. R. A. *Solid State Ionics* **2003**, *159*, 21–23.
(23) Launay, M.; Boucher, F.; Gressier, P.; Ouvrard, G. *J. Solid State Chem.* **2003**, *176*, 556–566.
(24) Wolverton, C.; Zunger, A. *J. Electrochem. Soc.* **1998**, *145*, 2424–2431.
(25) Courtney, I. A.; Tse, J. S.; Mao, O.; Hafner, J.; Dahn, J. R. *Phys. Rev. B* **1998**, *58*, 15583–15588.
(26) Meng, Y. S.; Wu, Y. W.; Hwang, B. J.; Li, Y.; Ceder, G. *J. Electrochem. Soc.* **2004**, *151*, A1134−A1140.
(27) Arroyo y de Dompablo, M. E.; Van der Ven, A.; Ceder, G. *Phys. Rev. B* **2002**, *66*, 064112.
(28) Arroyo y de Dompablo, M. E.; Ceder, G. *J. Power Sources* **2003**, *119−121*, 654–657.
(29) Carlier, D.; Ven, A. V. d.; Delmas, C.; Ceder, G. *Chem. Mater.* **2003**, *15*, 2651–2660.
(30) Reed, J.; Ceder, G. *Electrochem. Solid-State Lett.* **2002**, *5*, A145−A148.
(31) Kang, K.; Ceder, G. *Phys. Rev. B* **2006**, *74*, 094105.
(32) Koudriachova, M. V.; Harrison, N. M.; de Leeuw, S. W. *Phys. Rev. B* **2002**, *65*, 235423.
(33) Tibbetts, K.; Miranda, C. R.; Meng, Y. S.; Ceder, G. *Phys. Rev. B* **2007**, *76*, 16435.
(34) Perdew, J. P.; Burke, K.; Ernzerhof, M. *Phys. Rev. Lett.* **1996**, *77*, 3865.
(35) Blochl, P. E. *Phys. Rev. B* **1994**, *50*, 17953.
(36) Kresse, G.; Joubert, J. *Phys. Rev. B* **1999**, *59*, 1758.
(37) Kresse, G.; Furthmuller, J. *Phys. Rev. B* **1996**, *54*, 169.

full relaxation of the atomic positions and cell parameters for each structure. Ferromagnetic (FM), spin-polarized configurations were used for all Fe-containing structures though both iron trifluoride (FeF_3) and iron difluoride (FeF_2) are known to display antiferromagnetic (AFM) ground states below the Néel temperature (T_N), 363 and 79 K, respectively.[38–40] The AFM state is well below room temperature (RT) for FeF_2, and recent findings indicate that T_N drops to 39 K for FeF_3 as the crystallite size is reduced to amorphous nature,[41] so the FM configuration may not result in significant error. It should also be noted that the spin-magnetic moment obtained with FM configuration (e.g., $FeF_2 = 3.70\ \mu_B/Fe^{2+}$) is in good agreement with both AFM GGA calculations by other authors (e.g., $FeF_2 = 3.51\ \mu_B/Fe^{2+}$)[42] and the experimental value (e.g., $FeF_2 = 3.75\ \mu_B/Fe^{2+}$).[43] The total energy of F, used to derive the ternary phase diagram defined by Li, Fe, and F at 0 K, was determined from the experimental reaction enthalpy obtained for

$$Mg + F_2 \rightarrow MgF_2 \qquad (4)$$

and the calculated energies for Mg and MgF_2. This enables the total energy of fluorine to be determined by fitting the total energies of an insulator (i.e., MgF_2) and a nontransition metal (i.e., Mg) to the experimental reaction enthalpy and minimizes ab initio errors arising from the metal to anion charge transfer.[44]

FeF_3 possesses a trigonal structure with *R*-3*c* space group symmetry (S.G. no. 167), which is common to the majority of 3d metal trifluorides.[45] The hexagonal representation of the lattice, shown in Figure 1A, is composed entirely of corner-sharing $FeF_{6/2}$ octahedra. It is akin to the ABX_3 cubic perovskite wherein the "A" site cation has been removed, yielding a collapsed BX_3 structure in which the M−F−M bond angle has decreased from the ideal 180° (i.e., that observed for ReO_3 structure). As a result of the "A" site cation vacancy, continuous channels form along the **a** and **b** vectors of the unit cell, which result in vacant planes parallel to the (012) plane of $FeF_{6/2}$ octahedra in the hexagonal setting. Because of the relatively small ionic radii[46] for Li^+ (i.e., 0.59 Å for 4-fold coordination and 0.76 Å for 6-fold coordination) it is reasonable to expect that these channels can accommodate up to one Li^+ per FeF_3 formula unit via topotactic insertion.

The majority of 3d metal difluorides, including FeF_2, display a tetragonal structure with space group symmetry $P4_2/mnm$ (S.G. no. 136).[45] This structure, shown in Figure 1B, is of the rutile type and is composed of an hcp anion lattice with cations occupying half of the octahedral sites to form $FeF_{6/3}$ octahedra. These octahedra link in an edge-sharing manner along the [001] to form alternating chains of $FeF_{6/3}$ octahedra and vacant channels. The channels along the [001] can reasonably be expected to accommodate Li^+ coordinated in either tetrahedral or octahedral sites. However, Li^+ insertion into the most common form of rutile, TiO_2, has been found to be quite difficult due to strong anisotropic effects from Li−Li interaction in the crystal structure upon increasing Li^+ concentration.[32,47,48] In addition, TiO_2 makes use of the Ti^{4+}/Ti^{3+} couple, whereas initial Li^+ insertion into FeF_2 is restricted because Fe^{2+} reduction is required. For Li^+ insertion to occur, some Fe^{2+} would need to be reduced to either Fe^{1+} or disproportionation to Fe^0 and Fe^{3+} would need to take place. In general, solid-state Fe^{1+} is very unlikely and oxidation states <2+ are uncommon for elements of the first transition series unless a π-acid-type ligand (e.g., CO and NO) is present, or in some organometallic compounds.[49] If disproportionation occurs, combining some Fe^{2+} reduction to Fe^0 with some Fe^{2+} oxidation to Fe^{3+}, then metallic iron would likely precipitate out of the iron fluoride structure. Therefore, this mechanism would not be a strict insertion reaction because it requires an exchange of iron with lithium. During this process it would be possible for Li^+ to either fill an interstitial site in the channels, occupy the site that Fe^0 is removed from, or occupy space that is a combination of both limits. Additional possibilities exist such as charge-compensated aliovalent exchange, in which two Li^+ exchange for one Fe^{2+} of the rutile structure.

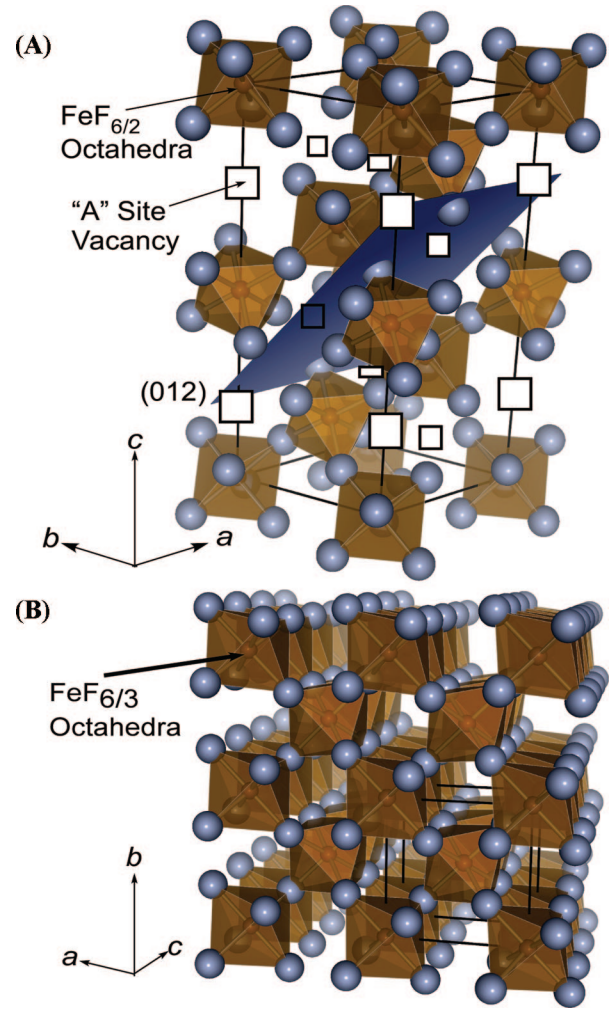

Figure 1. Panel A depicts the hexagonal representation of the FeF_3 unit cell with 6*a* site vacancies parallel to the (012) plane. Panel B illustrates the rutile structure of FeF_2, highlighting the vacant channels along the [001]. The unit cell is outlined in solid, black lines for each lattice.

As illustrated by the above discussion of the FeF_2 structure, the variety of possibilities in which a structure can be altered during a

(38) Strempfer, J.; Rutt, U.; Bayrakci, S. P. *Phys. Rev. B* **2004**, *69*, 014417.
(39) Wollan, E. O.; Child, H. R.; Koehler, W. C.; Wilkinson, M. K. *Phys. Rev.* **1958**, *112*, 1132.
(40) Erickson, R. A. *Phys. Rev.* **1953**, *90*, 779–785.
(41) Greneche, J. M.; Le Bail, A.; Mosset, A.; Varret, F.; Galy, J.; Ferey, G. *J. Phys. C: Solid State Phys.* **1988**, *21*, 1351–1361.
(42) Dufek, P.; Blaga, P.; Sliwko, V.; Schwarz, K. *Phys. Rev. B* **1994**, *49*, 10170.
(43) Brown, P. J.; Figgis, B. N.; Reynolds, P. A. *J. Phys.: Condens. Matter* **1990**, *2*, 5297.
(44) Wang, L.; Maxisch, T.; Ceder, G. *Phys. Rev. B* **2006**, *73*, 195107.
(45) Portier, J. *Angew. Chem.* **1976**, *15*, 475.
(46) Shannon, R. D. *Acta Crystallogr., Sect. A* **1976**, 32.
(47) Jiang, C.; Honma, I.; Kudo, T.; Zhou, H. *Electrochem. Solid-State Lett.* **2007**, *10*, A127−A129.
(48) Kavan, L.; Fattakhova, D.; Krtil, P. *J. Electrochem. Soc.* **1999**, *146*, 1375–1379.
(49) Cotton, F. A.; Wilkinson, G.; Murillo, C. A.; Bochmann, M. *Advanced Inorganic Chemistry*; 6th ed.; John Wiley & Sons, Inc.: New York, 1999.

Table 1. A Significant Number of Computations Have Been Conducted in Order to Survey the Great Variety of Theoretically Possible Structures That May Exist as Reaction Intermediates of the Li−Fe−F Ternary System

structural basis for calculation	no. of compounds calculated
perovskite-related Li_xFeF_3	∼40
Fe/Li exchange in FeF_2	∼10
FeF_3 partial insertion/exchange	∼10
FeF_2 partial insertion/exchange	∼25
spinel- and olivine-type Li_2FeF_4 compositions	∼15
LiF substituted with Fe	∼15

conversion reaction makes the search for thermodynamically stable lithiated structures significantly more difficult than predicting structures based strictly upon Li^+ insertion into interstitial sites. Table 1 illustrates the various approaches undertaken in this paper to determine stable, lithiated phases of iron fluoride. More than 100 compounds have been computed in order to investigate the probability of not only Li^+ insertion into FeF_3 (i.e., filling interstitial space) and direct FeF_2 conversion (i.e., exchanging iron for lithium) but also the possibility of reaction intermediates resulting from both partial lithium insertion and conversion. Additionally, LiF supercells containing minimal amounts of substituted iron were constructed in an effort to find the intermediates one might expect upon initial reconversion. A variety of compositions based on spinel and olivine structures have also been examined because of their close structural relation to rocksalt (e.g., LiF) and because consultation of structure−field maps for ternary compounds[50] indicates that these may be favorable structures based on ionic radii of lithium and iron.

III. Li−Fe−F Ternary Phase Diagram and the Equilibrium Reaction Path

The ternary Li−Fe−F phase diagram (plotted with LiF on one vertex, rather than Li, to focus on the relevant area) is presented in Figure 2. This plot has been constructed using the structure with lowest energy at each composition. The compositions marked by filled circles are part of the convex lowest energy hull, indicating that they are overall stable and have lower energy than any linear combination of other structures that add up to the same composition. In a ternary phase diagram at zero K, the phase regions are triangles indicating coexistence of three phases. At the compositions marked with an "×," inside a stable three-phase triangle, one or more structures were calculated but found to have higher energy than a mixture of the three compounds that define the triangle. Although such compounds are therefore thermodynamically unstable, they can be metastable if diffusion of some components is not fast enough to form the stable phases or if there are nucleation limitations for some of the compounds. Given that the chemical potential of all species is constant in each three-phase equilibrium region the Li chemical potential and voltage can be calculated as function of composition. For instance Figure 2 shows that any composition within the tie-triangle formed by LiF, Fe, and $Li_{1/2}FeF_3$ will possess a potential of 2.91 V versus Li metal under equilibrium conditions. All of the other three-phase regions have higher Li potentials. A potential for the three-phase equilibria connecting to pure F (shaded in gray)

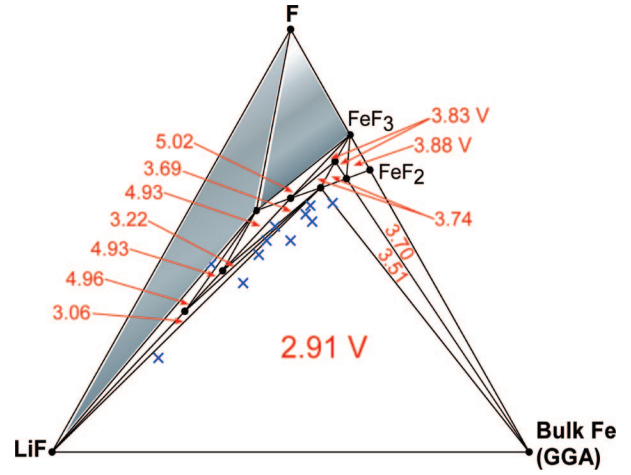

Figure 2. Phase diagram defined by Li, Fe, and F calculated from the lowest energy structures determined by first-principles computations. LiF is used as a vertex for ease of viewing the region of interest (e.g., the reaction path of iron fluoride conversion) although these plots represent the Li−Fe−F system. Thermodynamically stable structures are indicated by a filled circle while unstable structures are denoted with an "×." The lithium equilibrium potential is indicated for each three-phase region except for the two triangles that contain pure fluorine. The search for stable compositions within these two regions was insufficient and therefore yielded a significant degree of uncertainty in the corresponding potential.

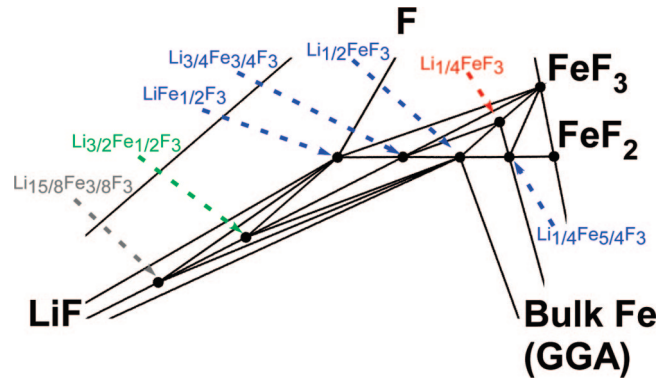

Figure 3. Expanded view of the calculated phase diagram identifying the compositions of the stable phases and their connecting tie lines. The stable lithiated fluorides include structures related to perovskite (red), rutile (blue), ilmenite (green), and spinel (gray).

is not given as we did not systematically search for stable structures in this composition space where the valence state of Fe would be very large.

An expanded view of the phase diagram area containing the relevant stoichiometries is presented in Figure 3, while the crystallographic information for the optimized structures of the lithiated iron fluorides is presented in Table 2. The experimentally observed structures, rocksalt, rutile, and distorted perovskite, were utilized for the binaries LiF, FeF_2, and FeF_3, respectively. The only experimentally known ternary compound within the Li−Fe−F system to have been directly synthesized is a trirutile of composition $Li_{1/2}FeF_3$;[51] however, another experimental effort indicated that electrochemical formation of Li_xFeF_3 (via Li^+ insertion into FeF_3) is also possible when $x \leq 1$.[13] Results of our study do indicate that Li^+ insertion into FeF_3 forms thermodynamically stable structures, but only up to about $x = 0.25$ as

(50) Muller, O.; Roy, R. *Crystal Chemistry of Non-Metallic Materials*; Springer-Verlag: New York, 1974.

(51) Portier, J.; Tressaud, A.; de Pape, R.; Hagenmuller, P. *C. R. Chim., Ser. C* **1968**, *267*, 1711–1713.

Table 2. Crystallographic Information of the Ternary Phases Predicted for the Li−Fe−F System and the Defect Trirutile FeF_3 Predicted as the Reconversion Product

Optimized Lattice Parameters Obtained From Total Energy Calculations									
		lattice parameters						atomic positions	
compd	space group	*a*, *b*, *c* (Å)	α, *β*, *γ* (deg)	*V* (Å^3)	prototype	atom	site	*x*, *y*, *z*	occupancy
$Li_{1/4}FeF_3$	derived from *R*-3*cR* (no. 167)	$a = 5.531$	$\alpha = 56.2$	108.88	derived from FeF_3	Li	2*a*	0.796, 0.786, 0.795	0.25
		$b = 5.528$				Fe	2*b*	−0.001, −0.009, −0.014	1
		$c = 5.518$				F	6*e*	0.857, 0.630, 0.244	1
$Li_{1/4}Fe_{5/4}F_3$	derived from $P4_2/mnm$ (no. 136)	$a = 4.820$	$\alpha = 90.0$	218.88	derived from $ZnSb_2O_6$	Li	2*a*	0, 0, 0	0.5
		$c = 9.421$	$\gamma = 89.3$			Fe	2*a*	0, 0, 0	0.5
						Fe	4*e*	0, 0, 0.326	1
						F	4*f*	0.293, 0.293, 0	1
						F	8*j*	0.301, 0.301, 0.333	1
$Li_{1/2}FeF_3$	$P4_2/mnm$ (no. 136)	$a = 4.756$	$\alpha = 90.0$	211.23	$ZnSb_2O_6$	Li	2*a*	0, 0, 0	1
		$c = 9.339$				Fe	4*e*	0, 0, 0.334	1
						F	4*f*	0.305, 0.305, 0	1
						F	8*j*	0.299, 0.299, 0.329	1
$Li_{3/4}Fe_{3/4}F_3$	$P12_1/c1$ (no. 14)	$a = 5.625$	$\alpha = 90.0$	138.77	$LiMnF_4$	Fe	2*a*	0, 0, 0	1
		$b = 4.774$	$\beta = 114.4$			Li	2*d*	0.5, 0.5, 0	1
		$c = 5.676$	$\gamma = 90.0$			F	4*e*	0.855, 0.792, 0.662	1
						F	4*e*	0.327, 0.687, 0.635	1
$LiFe_{1/2}F_3$	$P4_2/mnm$ (no. 136)	$a = 4.728$	$\alpha = 90.0$	199.14	$ZnSb_2O_6$	Fe	2*a*	0, 0, 0	1
		$c = 8.908$				Li	4*e*	0, 0, 0.342	1
						F	4*f*	0.288, 0.288, 0	1
						F	8*j*	0.313, 0.313, 0.348	1
$Li_{3/2}Fe_{1/2}F_3$	*R*3*H* (no. 146)	$a = 5.102$	$\alpha = 90.0$	314.30	Ni_3TeO_6	Fe	3*a*	0, 0, 0.846	1
		$c = 13.940$	$\gamma = 120.0$			Li	3*a*	0, 0, 0.146	1
						Li	3*a*	0, 0, 0.355	1
						Li	3*a*	0, 0, 0.643	1
						F	9*b*	0.325, 0.018, 0.249	1
						F	9*b*	0.701, 0.003, 0.754	1
$Li_{15/8}Fe_{3/8}F_3$	$P4_332$ (no. 212)	$a = 8.415$	$\alpha = 90.0$	595.86	$LiFe_5O_8$	Fe	4*b*	0.625, 0.625, 0.625	1
						Li	8*c*	−0.003, −0.003, −0.003	1
						Li	12*d*	0.125, 0.393, 0.867	1
						F	8*c*	0.380, 0.380, 0.380	1
						F	24*e*	0.130, 0.870, 0.141	1
defect trirutile FeF_3	derived from $P4_2/mnm$ (no. 136)	$a = 4.942$	$\alpha = 90.0$	216.09	derived from $ZnSb_2O_6$	vacant	2*a*	0, 0, 0	0
		$c = 8.846$				Fe	4*e*	0, 0, 0.324	1
						F	4*f*	0.176, 0.824, 0.500	1
						F	8*j*	0.217, 0.783, 0.184	1

indicated by the color coding in Figure 3. In addition, we observe from the calculated crystal structures that it is significantly more energetically favorable to shift Li^+ off the "A" site of the FeF_3 perovskite enabling it to occupy roughly half the interstitial space of each "A" site. In doing so the Li^+ becomes octahedrally coordinated and shares a single face with an adjacent Fe-centered octahedra. At composition $Li_{1/2}FeF_3$ the trirutile structure yields a slightly more favorable energy (∼25 meV/atom) than the best structure we could find that has Li^+ inserted topotactically into perovskite FeF_3. This energy difference is small enough that it could be overcome by entropy effects at finite temperature or by minor polarization of the Li potential. Additional, thermodynamically stable, rutile structures (i.e., $Li_{1/4}Fe_{5/4}F_3$, $Li_{3/4}Fe_{3/4}F_3$, and $LiFe_{1/2}F_3$) were generated by substituting iron for lithium in a one-for-one manner in FeF_2, thus creating an increasingly "converted" FeF_2 structure. Such one-for-one Li/Fe substitution creates structures with increasing valence of Fe. Figure 4A depicts the unit cell of $Li_{3/4}Fe_{3/4}F_3$, one example of the exchanged rutiles. This is the composition in which half the cation sites contain lithium while the remaining sites contain iron. Parts B and C of Figure 4 depict two other previously unknown phases of the Li−Fe−F system, a corundum-like structure at $Li_{3/2}Fe_{1/2}F_3$ and the spinel-like $Li_{15/8}Fe_{3/8}F_3$, respectively. $Li_{3/2}Fe_{1/2}F_3$ displays the *R*3*H* (no. 146) space group of prototype Ni_3TeO_6. This compound can be related to corundum, Al_2O_3, by replacing Al with Li and Fe ordered in the 3*a* site. It can also be related to ilmenite, $FeTiO_3$, because of the similar cation ordering. However, it is an iron-deficient ilmenite because the Li/Fe ratio is 3:1, rather than the 1:1 Fe/Ti ratio observed in the prototype. Although structurally different from $Li_{3/2}Fe_{1/2}F_3$, the inverse spinel, $Li_{15/8}Fe_{3/8}F_3$, is also iron-deficient with respect to the standard A_2BX_4 composition of spinel. The structure of $Li_{15/8}Fe_{3/8}F_3$ possesses the symmetry of the space group $P4_332$ (no. 212) with the prototype $LiFe_5O_8$. More detailed discussion of the importance of these structures and their relation to the electrochemical reaction is presented in section V.

The theoretical voltage profile for reaction of FeF_3 with Li can be deduced from the phase diagram and the Li potentials in each three-phase triangle. Discharging FeF_3 by adding Li causes the overall composition point to move along the line between FeF_3 and Li. The equilibrium reaction path is highlighted in the expanded phase diagram as shown in Figure 5B, and the voltage profile is shown in Figure 5A. The calculations indicate that Li^+ insertion into perovskite FeF_3 is the most favorable initial reaction mechanism, up to at least $Li_{1/4}FeF_3$, after which a transformation to the trirutile at $Li_{1/2}FeF_3$ may occur, though further Li insertion is very

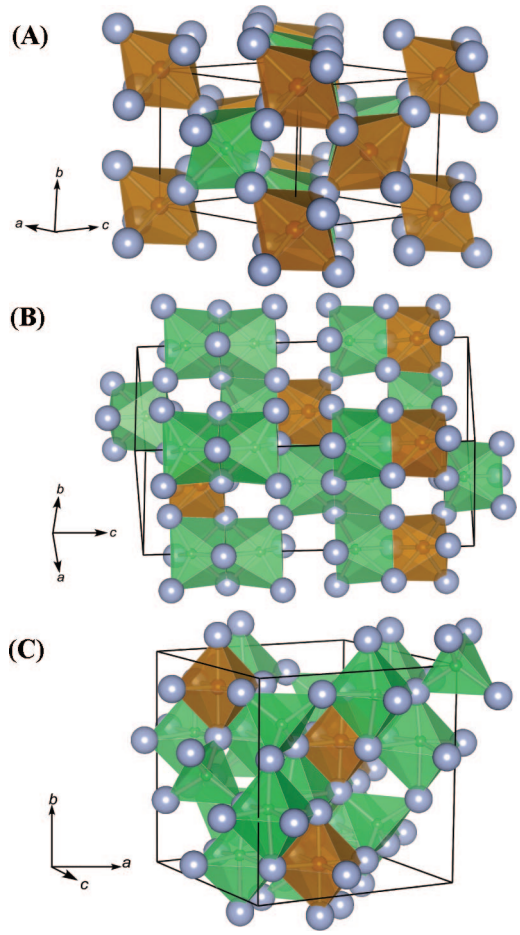

Figure 4. Unit cells for three previously unidentified phases of the Li−Fe−F system. Panel A depicts $Li_{3/4}Fe_{3/4}F_3$, one of several lithiated rutile structures found during this investigation ($Li_{1/2}FeF_3$ is the only previously known example for the Li−Fe−F system). Panel B corresponds to $Li_{3/2}Fe_{1/2}F_3$, an ilmenite-related structure, while the spinel-related $Li_{15/8}Fe_{3/8}F_3$ is shown in panel C. Lithium-centered polyhedra are shown in green, while iron-centered polyhedral are brown, and each unit cell is outlined in black.

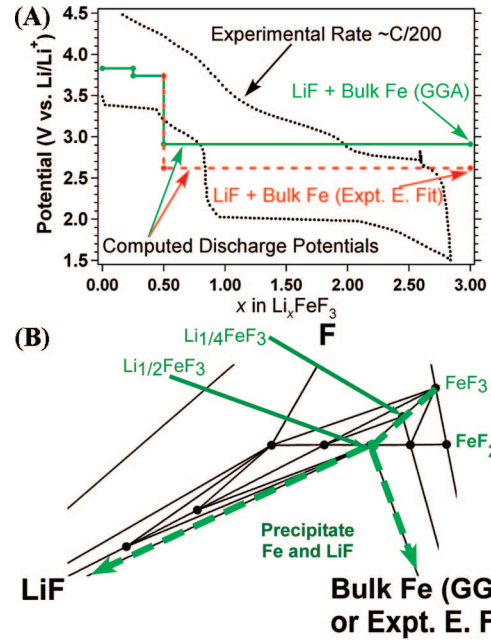

Figure 5. Calculated equilibrium potential profile obtained with the GGA computed energy of bulk Fe (green, solid line) is depicted in panel A. The decrease in potential, between $x = 0.5$ and $x = 3$ in Li_xFeF_3, obtained by fitting the Fe energy to experiment is shown in panel A as a red, dashed line. Panel A also contains the experimental voltage profile for the first cycle of an FeF_3/C nanocomposite (black, dotted line). The data was collected under constant current conditions at a rate of *C*/200. It was provided to us by Professor Glenn Amatucci of Rutgers, The State University of New Jersey. The equilibrium reaction path associated with the calculated equilibrium potential profile is highlighted (green, dashed arrows) on the phase diagram in panel B.

competitive since the Li-inserted FeF_3 at the same composition is only 25 meV/atom higher in energy. Given the kinetic ease of Li insertion, compared to the rearrangements needed to form trirutile, it seems reasonable that in experiments Li^+ insertion is still observed at $x = 0.5$ in Li_xFeF_3. The calculated equilibrium profile indicates that further lithiation causes the intermediate phase, $Li_{1/2}FeF_3$, to disproportionate into Fe and LiF, rather than undergo continued Li^+ insertion.

IV. Deviation between Calculated and Experimental Potential

In a complex multiphase conversion system such as the FeF_3−Li system, there are many reasons why calculated equilibrium potentials may differ from experimentally observed charge and discharge potentials. Polarization, deviation from the equilibrium path, or nano effects, and intrinsic errors in our first-principles energy method (GGA) can all play a role in the difference between the calculated and experimental potential displayed in Figure 5. We will discuss several of these in turn and propose a model for the nonequilibrium reaction path.

The conversion step from Li_xFeF_3 to LiF and Fe involves the reduction of ionic Fe to metallic Fe. It is well-established that due to its spurious self-interaction the GGA prediction error grows as materials are compared in which the electron states are very different.[19] For this reason GGA does not capture well the energy difference between the localized d-states for ionic iron in an oxide or fluoride and the delocalized states in metallic iron.[42,52] For the purpose of our phase diagram calculations this problem can be solved by simply determining the energy of metallic Fe from the experimentally measured reaction enthalpy obtained for

$$FeF_2 + 2Li \rightarrow Fe + 2LiF \qquad (5)$$

and the calculated energies for Li, FeF_2, and LiF. This enables the total energy of bulk iron to be determined by fitting the total energies of two insulators (i.e., FeF_2 and LiF) and a nontransition metal (i.e., Li) to the experimental reaction enthalpy. This approach yields a cohesive energy of −4.3447 eV for bulk, metallic iron, only ~65 meV lower than that obtained from experiment[53] (i.e., −4.28 eV), and ensures that the energy difference between oxidized Fe and metallic Fe is well-represented in the calculations. Utilizing the fitted energy of Fe to calculate the reaction potential reduces the potential of conversion from 2.91 to 2.62 V (Figure 5A).

All calculations in Figure 5 are for bulk compounds, whereas reasonable Li reaction rates can only be obtained for nanoparticles. As Fe precipitates out from the fluoride

(52) Tran, F.; Blaha, P.; Schwarz, K. *Phys. Rev. B* **2006**, *74*, 155108.
(53) Philipsen, P. H. T.; Baerends, E. J. *Phys. Rev. B* **1996**, *54*, 5326–5333.

matrix it is likely to form very small clusters. It is well-known that the cohesive energy of very small particles is significantly reduced from the bulk value.[54,55] Although a full investigation of the Li−Fe−F phase space at nanoscale dimensions is outside the scope of the work presented in this paper we calculated the energy of a 1 nm spherical particle of bcc iron to assess the nanosize effect. The total energy was obtained in a manner similar to other nanoscale calculations presented in the literature[55] and internally consistent with the bulk calculations in this work (e.g., full relaxation of atomic positions, planewave cutoff of 550 eV, etc., except that this computation utilized the Γ-point *k*-space integration only). The calculated cohesive energy of the 1 nm Fe particle is −4.0545 eV, a significant change from the −5.0713 eV obtained with GGA computation of bulk Fe. To remain consistent by accounting for the inherent error within the GGA method, the nanoparticle energy was also corrected by the same amount as the bulk energy in the previous section. This yields a cohesive energy of −3.3279 eV for fitted nanoscale Fe, a value that corresponds well with the trend expected for embedded nanoparticles within this size range.[54]

Figure 6A shows the voltage profile when the energy of nanoscale Fe is used in the reaction energy. Both the pure first-principles voltage (GGA) and the "corrected" potential are given. Lithiation of FeF_3 is unchanged from the bulk phase up to $x = 0.5$ by the introduction of nanosize Fe. However, lithiation beyond $x > 0.5$ moves the system through several smaller three-phase triangles, before Fe precipitation occurs. Both the correction and the nanosized form of Fe lead to increase the energy of Fe (reduce its cohesive energy). This increase stabilizes compounds with higher Li-to-Fe ratio in the phase diagram. In particular, the lithiation path now crosses three-phase triangles connecting $Li_{1/4}Fe_{5/4}F_3$ and $Li_{3/2}Fe_{3/4}F_3$ with LiF, and FeF_2 with $Li_{1/4}Fe_{5/4}F_3$ and $Li_{3/2}Fe_{3/4}F_3$. Many of these reactions are nonintuitive if one is used to thinking of conversion reactions in binary systems. For example, consider the first reaction for $x > 0.5$ in which LiF and $Li_{1/4}Fe_{5/4}F_3$ form. This reaction may seem surprising at first since the Fe-to-F ratio increases in $Li_{1/4}Fe_{5/4}F_3$ from FeF_3. However, this reaction could rather easily occur by reaction of Li and F at the surface and diffusion of Fe from the surface of the particle toward the interior. After this reaction, the GGA nanopath (with uncorrected Fe energy) leads to precipitation of Fe. However, in the path using the fitted energy for Fe, the higher energy of Fe delays the precipitation and several other complex three-phase triangles cause further conversion reactions between various Li−Fe−F compounds before metallic Fe is formed. Surprisingly, under this scenario, it is even possible that FeF_2 forms along the reaction path. The stabilization of more intermediate phases in the phase diagram also modifies the voltage profile (Figure 6A). Following the path defined in Figure 6B (red, dashed line), the voltage profile where we use nanosized Fe with experimentally based correction agrees remarkably well with

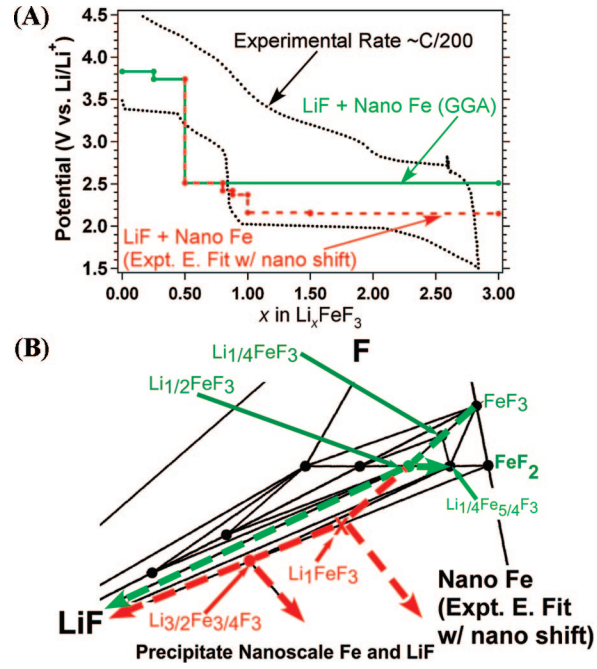

Figure 6. Panel A depicts the voltage profile for iron fluoride conversion when accounting for the energy of GGA computed nanoscale Fe (green, solid line) while the red, dashed line corresponds to the fitted energy of Fe, which is shifted by the energy difference between GGA computed bulk and nanoscale Fe. The experimental profile is also displayed as a black, dotted line. Panel B highlights the corresponding reaction paths of iron fluoride conversion. This is depicted as green, dashed arrows when accounting for the energy of GGA computed nanoscale Fe, while the red, dashed arrows correspond to the fitted energy of Fe, which is shifted by the energy difference between GGA computed bulk and nanoscale Fe. Note that applying the energy difference between bulk and nanoscale Fe (obtained with GGA) to the energy of Fe obtained by fitting to experiment yields $Li_{3/2}Fe_{3/4}F_3$ as a stable structure, creating additional tie line from $Li_{3/2}Fe_{3/4}F_3$ to each LiF, FeF_2, and $Li_{1/4}Fe_{5/4}F_3$.

the experimental data. Some discrepancy between the calculated and experimental voltage profile does remain, particularly between $x = 0.5$ and $x = 1$ in Li_xFeF_3. There are several possible reasons for this discrepancy. Other stable phase(s) in this concentration range may decrease the predicted voltage drop. Even though we searched extensively for stable structures in this region we were unable to find any, which may be indicative that no such stable phase(s) form between $Li_{1/2}FeF_3$ and Li_1FeF_3. It is of course always possible that our search was not exhaustive enough. Another possibility is that the kinetic limitation on Fe diffusion in the fluoride delays the precipitation of Fe until the composition Li_1FeF_3 is reached. Some arguments can be made to this effect by comparing the experimental and calculated voltage curve over the complete range of $0 < x < 1$ and noting that the *average* over this voltage range is in better agreement with experiments than the actual curve. The average voltage between $x = 0$ and $x = 1$ is only determined by the energy of the $x = 0$ state (FeF_3) and the $x = 1$ state ($LiFeF_3$). For $0 < x < 0.5$ the experimental voltage curve is lower than the calculated one. This indicates that in the experiment the system evolves to a higher energy state for $Li_{1/2}FeF_3$ than in the calculation when Li is inserted. This could be due to Fe disorder which is induced by the Li insertion. In the second stage, for $0.5 < x < 1$ the higher energy state for $Li_{1/2}FeF_3$ leads to a lower voltage when further discharging to $LiFeF_3$.

(54) Cao, L. F.; Xu, G. Y.; Xie, D.; Guo, M. X.; Luo, L.; Li, Z.; Wang, M. P. *Phys. Status Solidi B* **2006**, *243*, 2745–2755.
(55) Rollmann, G.; Gruner, M. E.; Hucht, A.; Meyer, R.; Entel, P.; Tiago, M. L.; Chelikowsky, J. R. *Phys. Rev. Lett.* **2007**, *99*, 083402−083405.

Some of the new phases that are predicted to be stable (or metastable) along the reaction path may be particularly significant. The compound at composition $Li_{3/2}Fe_{3/4}F_3$ has an inverse spinel structure in which Li^+ occupies all the tetrahedral sites and half the octahedral cation sites while Fe^{2+} occupies the remaining octahedral sites. Note that the prediction of stable $Li_{3/2}Fe_{3/4}F_3$ makes $LiFeF_3$ metastable (Figure 6B); however, the compound is indicated on the phase diagram as it may form if no Fe migration can occur.

V. Model for the Nonequilibrium Reaction Path

V.A. Conversion. Conversion reactions almost always display significant polarization (difference between charging and discharging voltage). To discuss this it may be useful to distinguish classical polarization including ohmic effects and diffusion polarization from changes in potential related to the fact that the system may strongly deviate from its equilibrium path in the phase diagram and go through different phases upon charge and discharge. Since the traditional polarization depends to some extent on the morphology and design of the composite electrode in which the active material is embedded, we do not treat it here and instead focus on the polarization caused by the system deviating to a nonequilibrium path through the phase diagram. The formation of different phases in charge and discharge would show up as hysteresis that is intrinsic to the active material and, as such, would be unaffected by the traditional enhancements used to improve rate such as large carbon additions or the use of thin film electrodes. Phase hysteresis is caused by the fact that, at low temperatures, structures often convert to the reaction product that is most easily reached kinetically, rather than to the thermodynamic ground state. This kinetic phase sequence is not reversible and will be distinct in charge and discharge.

One can think of the reaction with Li and FeF_3 (or more exactly Li_xFeF_3 with $x \approx 1$) as an interdiffusion problem. Either Li has to diffuse into the fluoride host while Fe diffuses out and precipitates, or F has to migrate between the FeF_3 and Li. It is well-known that in ternary systems, the intermediate compositions between two interdiffusing phases do not necessary interpolate linearly between the composition of these phases but can follow a very curved path in the ternary diagram, depending on the relative diffusivity of each species.[56] The reason is that the faster moving species will at all times want to equilibrate itself, even against a nonequilibrium distribution of the slower moving species.

We can speculate on what the kinetic path may be under different assumptions regarding the relative diffusivity of Fe and Li. Starting with the least likely scenario, if the diffusivity of Li is much less than that of Fe during conversion, then Fe will equilibrate for any concentration (and chemical potential of Li), and the reaction should proceed along the thermodynamic equilibrium path as determined by the phase diagrams in Figures 5B and 6B (green, dashed lines). Hence, Fe would precipitate out from Li_xFeF_3 as soon as the amount of Li in the compound reaches the equilibrium concentration. The maximal reduction of Fe in Li_xFeF_3 in this model depends on the solubility limit of Li in Li_xFeF_3 in equilibrium with LiF and Fe. The more plausible scenario is that the diffusivity of Fe is significantly less than the diffusivity of Li. In this case we should expect that Li will accumulate easily within Li_xFeF_3 thereby reducing Fe to the maximum possible extent (i.e., entirely Fe^{2+}) prior to precipitation of metallic iron. This is an example of a kinetically chosen path: rather than extrude metallic Fe, which is slow and possibly associated with a large overpotential, Li inserts in the compound until all Fe is reduced to Fe^{2+}, the lowest valence state that it can be expected to have in an ionic material. In Figure 6A (red, dashed line) we plot the voltage associated with a reaction path that gives maximal reduction to Fe^{2+} in the fluorides and only then precipitates Fe. Under these assumptions, we find the following reaction path (shown as red, dashed line in Figure 6B) in which FeF_3 lithiates to $LiFeF_3$ by undergoing topotactic insertion followed by some cation rearrangement to minimize face-sharing between Fe and Li octahedra within the $LiFeF_3$ structure. Note that such cation rearrangement may take place even when the Fe mobility is low as the migration distances for rearrangement of Li and Fe in the host are only a few angstroms, versus the several tens of nanometers required for Fe precipitation. Subsequently $LiFeF_3$ becomes $Li_{3/2}Fe_{3/4}F_3$, and then LiF, by precipitating nanoscale Fe while incorporating more Li. Essentially the reaction should be expected to continue through phase space associated with the lithiation path formed by the tie line connecting FeF_3 to $LiFeF_3$. Subsequently, the need to precipitate Fe^{2+} from $LiFeF_3$, so as to continue accommodating Li^+, will push the composition of intermediates toward phase space bounded by $Li_{3/2}Fe_{3/4}F_3$, LiF, and Fe. Regardless of the exact intermediate compositions, the potentials associated with the phase space for this portion of the reaction, $x = 1$ to $x = 3$ in Li_xFeF_3, correspond to a voltage of ~2.15 V, which is in reasonable agreement with experimental measurements.[11]

V.B. Reconversion. If interdiffusion limitations are central to driving the conversion reaction into nonequilibrium phase space during discharge, then they are likely to have an analogous effect upon the reconversion reaction during charge. Similar to the arguments made for conversion, if the Fe diffusivity is significantly less than that of Li the reaction intermediate(s) will consistently be Fe-deficient relative to the amount of Li migrating out of the electroactive structure as Fe diffusion cannot keep up. Consequently, reconversion should promote the formation of phases containing the highest possible oxidation states of Fe as this path allows for the largest ratio of Li extraction to Fe insertion. With this principle, a reconversion reaction path and voltage profile can be estimated. We limit oxidation of Fe in the fluoride compounds to Fe^{3+} because the phase space containing higher valence states corresponds to potentials of at least ~5 V versus Li/Li^+. Figure 7A shows (in blue) the computed nonequilibrium reconversion profile when oxidation to Fe^{3+} occurs as soon as Fe is taken up in the fluoride hosts. The reaction path and compositions of the intermediate phases

(56) Cohen, R. M. *Mater. Sci. Eng.* **1997**, *R20*, 167–280.

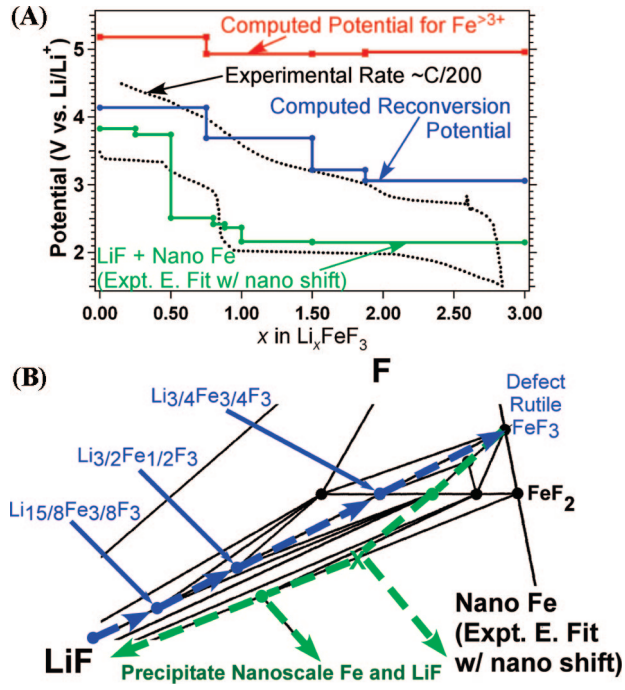

Figure 7. Panel A depicts the voltage profile for iron fluoride reconversion during charging (blue, solid line) as compared with the voltage profile for iron fluoride conversion when accounting for the energy of GGA computed nanoscale Fe (green, solid line) and the experimental profile (black, dotted line). The potentials required to form phases with $Fe^{>3+}$ during reconversion (red, solid line) are also presented. The corresponding reaction path is highlighted for discharge (green, dashed arrows) and charge (blue, dashed arrows) in panel B.

along this path are depicted in Figure 7B. For comparison, an alternative nonequilibrium reaction path allowing for oxidation of Fe beyond Fe^{3+} in the fluoride compounds is also shown (Figure 7A, in red). Clearly, this path is unrealistic as it requires very high charge potentials. Using the principle of oxidation to Fe^{3+} we find that delithiation proceeds through several new compounds highlighted along the (blue) path that begins with rocksalt-structured LiF. The structures along the reconversion path include $Li_{15/8}Fe_{3/8}F_3$, $Li_{3/2}Fe_{1/2}F_3$, and $Li_{3/4}Fe_{3/4}F_3$, which are, respectively, related to spinel, ilmenite, and rutile (structures shown in Figure 4). In general, each phase is iron-deficient with respect to the relevant prototype composition.

The evolution from the rocksalt LiF to the spinel-like $Li_{15/8}Fe_{3/8}F_3$ may be relatively easy as they have the same anion framework, and similar transitions have previously been observed during the lithiation process of several transition metal oxides including iron oxide.[57,58] The long-range cation ordering of the spinel composition observed in $Li_{15/8}Fe_{3/8}F_3$ is akin to that of $LiNi_{1/2}Mn_{3/2}O_4$[59] but yields an iron-deficient, inverse spinel. The stoichiometry of $Li_{15/8}Fe_{3/8}F_3$ can be rewritten as $Li(Fe_{1/2}Li_{3/2})F_4$ to illustrate its correspondence to a spinel. Li occupies the tetrahedral site, while Li and Fe share the octahedral sites.

Further conversion along our proposed nonequilibrium path would cause a transition from spinel to ilmenite and then to rutile. Such transitions are also found in systems other than Li−Fe−F: this structural path is of great importance to the Fe−Ti−O system in which the spinel/ilmenite/rutile transition corresponds to composition changes from Fe_2TiO_4 to $FeTiO_3$, and then to TiO_2, resulting from oxidative removal of iron.[60,61] In fact, studies examining the intergrowth of titaniferous spinel with ilmenite are of interest to geologists[62] in part because ilmenite and rutile are the greatest, natural source for production of titanium.[63] Like the spinel described above, both the ilmenite and rutile structures contain only Fe^{3+} and are iron-deficient when compared with respective prototype compositions that would be based on pure Fe−F compounds. For example, the ilmenite composition is $Li_{3/2}Fe_{1/2}F_3$, rather than $LiFeF_3$, and the rutile composition is $Li_{3/4}Fe_{3/4}F_3$, rather than $Fe_{3/2}F_3$.

The nonequilibrium path we predict from the principle of maximum Fe oxidation shows a reasonable resemblance to the measured voltage profile in charge, though there are some deviations. The fact that the calculated initial charge voltage is somewhat too high may be related to errors in the energy of metallic Fe (which is consumed in this step) or may reflect that in the beginning of charge full oxidation to Fe^{3+} in the fluoride is not necessary (i.e., it may be possible to form an Fe^{2+} intermediate phase, thus yielding lower observed voltage) as there is still a lot of Fe available near the surface of the LiF particles.

An interesting aspect of our predicted nonequilibrium reconversion path is that the last stable Li−Fe−F compound before full reconversion to FeF_3 is a rutile-related compound ($Li_{3/4}Fe_{3/4}F_3$). If exchange of one Fe^{3+} for three Li^+ should continue, from this compound along the easiest path, it is likely that rutile-like $Li_{3/4}Fe_{3/4}F_3$ will reconvert directly to a rutile-related FeF_3. Our first-principles computations indicate that this is quite possible by removing Li from $Li_{3/4}Fe_{3/4}F_3$ (and inserting Fe) to form a defect trirutile structure with a FeF_3 composition. The defect trirutile FeF_3 is only slightly (i.e., ~20 meV/atom) more unfavorable than the perovskite form of FeF_3. This observation supports the experimental finding that a structure related to FeF_2 forms upon completion of the charge process even though a capacity equivalent of approximately three Li^+ has been removed.[11] We suggest that what actually forms is the FeF_3 defect trirutile with the crystallographic parameters as detailed in Table 2. Because of the supercell nature of our calculations this is an ordered defect rutile, but it is possible that a more disordered defect rutile would be observed in experiments. A comparison of the calculated X-ray diffraction (XRD) spectra for rutile FeF_2 and the defect trirutile FeF_3 predicted by our calculations is displayed in Figure 8. Four peaks, shown to remain visible at the fine nanoscale,[11] are also labeled. Comparison of the peaks in these two spectra demonstrates that the defect trirutile and rutile may be virtually indistinguishable, par-

(57) Kanzaki, S.; Yamada, A.; Kanno, R. *J. Power Sources* **2007**, *165*, 403–407.
(58) Wu, E.; Tepesch, P. D.; Ceder, G. *Philos. Mag. B* **1998**, *77*, 1039–1047.
(59) Gryffroy, D.; Vandenberghe, R. E.; Legrand, E. *Mater. Sci. Forum* **1991**, *79−82*, 785–790.
(60) Reddy, S. N. S. *Metall. Mater. Trans. A* **2005**, *36A*, 2993–3000.
(61) Reddy, S. N. S.; Leonard, D. N.; Wiggins, L. B.; Jacob, K. T. *Metall. Mater. Trans. A* **2005**, *36A*, 2685–2694.
(62) Lattard, D. *Am. Mineral.* **1995**, *80*, 968–991.
(63) Chen, G. Z.; Fray, D. J.; Farthing, T. W. *Nature* **2000**, *407*, 361–364.

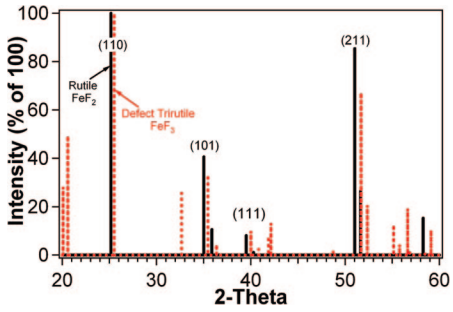

Figure 8. Calculated X-ray diffraction (XRD) spectra for rutile FeF_2 (solid, black line) and the defect trirutile FeF_3 (dashed, red line) found during the course of our investigation of the Li−Fe−F system. Four peaks known to remain visible in the nanocrystalline iron fluoride are indexed to show that these spectra should be essentially indistinguishable under such conditions.

ticularly when examined at the nanoscale because of the broad, low-intensity spectra that will be observed. However, the defect trirutile is consistent with the removal of three Li^+ and does not require explanations of the charge capacity through interfacial and nano effects.

VI. Discussion and Conclusions

We calculated the energy of a large amount of possible structures in the ternary Li−Fe−F system with first-principles methods in order to explore the system's phase diagram and the lithiation/delithiation reactions of iron fluorides. Several new stable compounds are found and predicted by the calculations. At compositions where the structure is known we confirm the stable crystal structure. We predict that the equilibrium reaction path of FeF_3 with Li consists of intercalation up to $Li_{1/4}FeF_3$. Further Li addition would lead—in equilibrium—to nontopotactic changes, and ultimately Fe precipitation, though topotactic lithiation is competitive in energy up to at least $Li_{1/2}FeF_3$. The voltage predicted along this equilibrium reaction path does not agree well with experimental observations. In particular the voltage at the final step in which Fe precipitates is considerably too high indicating that the energy of Fe as calculated is substantially lower than the energy at which Fe is formed in the experiment. There could be several causes for this. We investigated the accuracy of the calculations in predicting the Fe energy by comparing to known thermodynamic data of simple fluorides and found that it could only explain a small part of the discrepancy between experiments and calculations. By explicitly calculating the energy of a 1 nm Fe nanoparticle we find instead that most of the potential drop arises from the loss of cohesive energy when Fe forms at the nanoscale. Although one may think of this as a form of "overpotential" it is not a true polarization effect as recharging the Fe(nano) + LiF system can in principle occur at the same potential as the discharge. Instead, it should be thought of as a modification of the equilibrium potential by making one of the reaction products nanosized and may, therefore, be the first actual observation of the effect of particle size on the lithiation voltage.

We have also proposed a model for the large voltage hysteresis observed in experiments: the large difference in mobility that is expected between Fe cations and Li^+ in the fluoride host always causes the Fe concentration in the active part of the material to lag behind the equilibrium concentration for a given Li content (i.e., there is Fe excess during Li insertion and Fe deficiency upon Li extraction). We propose that upon Li insertion the easiest kinetic path is the one whereby all Fe is reduced to Fe^{2+} in the host—regardless of what the equilibrium reaction is—thereby maximizing the amount of Li that can be inserted before Fe needs to precipitate out. Upon reconversion (Li extraction), the effect of our kinetic assumptions is much more pronounced. To minimize the amount of Fe needed to compensate for Li extraction from LiF, all Fe that enters the fluoride material is oxidized to Fe^{3+}. Hence we predict that the reconversion path is essentially the lowest energy path that consists exclusively of LiF and $Li-Fe^{3+}-F$ compounds. The potential predicted along this path agrees quite well with the measured reconversion potential. Further credibility to our theory is provided by the fact that it predicts that an FeF_3 compound forms with a defect trirutile structure, consistent with experimental evidence from XRD spectra.

In our kinetic model the hysteresis is caused by the different paths through the phase diagram that the system takes upon charge and discharge. Although the concept of reversibility in thermodynamics requires both paths to be the same in equilibrium, the path that is kinetically most easy, taken under nonequilibrium conditions, can be significantly different for Li addition and Li extraction.

To test this theory of phase hysteresis, in situ diffraction experiments would be very valuable. In addition, the generality of our model remains to be proven by testing whether it can also explain the hysteresis in other conversion reactions.

Acknowledgment. This research was supported by the Intelligence Community Postdoctoral Research Fellowship Program award number HM1582-06-1-2012. The authors thank Geoffroy Hautier for helpful discussion and Professor Glenn Amatucci for providing the experimental data for comparison with our results. In addition, supercomputing resources were provided by the San Diego Supercomputing Center.

CM801105P